Giant Nonlinear Optical Response in 2D Perovskite Heterostructures

Jun Wang, Yang Mi, Xian Gao, Junzi Li, Junze Li, Shangui Lan, Chen Fang, Hongzhi Shen, Xinglin Wen, Rui Chen, Xinfeng Liu,* Tingchao He,* and Dehui Li*

2D layered halide perovskites have attracted significant attention. Apart from the linear optical properties, it is also intriguing to explore the non-linear optics of 2D layered halide perovskites and their heterostructures. Previous nonlinear optical (NLO) studies of 2D perovskites primarily focus on the thin films or microplates. Herein, the NLO properties of $(n\text{-}C_4H_9NH_3)_2PbI_4/(n\text{-}C_4H_9NH_3)_2(CH_3NH_3)Pb_2I_7$ heterostructures with centimeter size are systematically studied. The NLO properties can be continuously tuned by changing the thickness. A giant two-photon absorption (2PA) coefficient up to 44 cm MW^{-1} is obtained for the heterostructures with a total thickness of 20 μm based on the nonlinear transmittance measurement. Additionally, strong multiphoton-induced photoluminescence is observed in the heterostructures. It is proposed that the giant 2PA coefficient might arise from the small thickness ($\approx$1 μm) of $(n\text{-}C_4H_9NH_3)_2(CH_3NH_3)Pb_2I_7$ layer and possibly the nonradiative energy transfer between the different constituting layers within the heterostructures through an antenna-like effect. Finally, benefiting from the giant 2PA coefficient, direct detection of 980 nm light is demonstrated with a responsivity of 10^{-7} A W^{-1} in the heterostructures. The findings suggest the promising applications of 2D perovskite heterostructures in the infrared photodetection and some other nonlinear absorption related optoelectronic devices.

1. Introduction

3D organic–inorganic halide perovskites were initially studied in solar cells due to their ease of fabrication, low cost, and high power conversion efficiency (PCE).[1] The certified PCE has soared up to more than 23% in less than 10 years.[1b] Recently, the attention of organic–inorganic halide perovskites has gradually extended to a wide range of other optoelectronic devices including lasers, light-emitting diodes (LEDs), photodetectors, and memories.[2] Additionally, the nonlinear optical (NLO) properties of organic–inorganic halide perovskites have attracted increasing attention due to their large NLO response such as strong third-order NLO response and their potential applications in infrared photodetectors, multiphoton spectroscopy, and optical frequency converters by generating second or third harmonic signals.[3] For instance, organic–inorganic perovskite thin films show a strong third-order NLO response, whose third-order susceptibility is three orders of magnitude larger than that of silicon.[4] In addition, Sargent et al. have also demonstrated an infrared perovskite photodetector based on two-photon absorption (2PA) of the $CH_3NH_3PbBr_3$ bulk crystals.[3a]

3D organic–inorganic halide perovskites suffer from the fast degradation in ambient conditions, limiting their practical applications.[5] 2D Ruddlesden–Popper layered perovskites exhibit much better environmental stability over 3D organic–inorganic perovskites and thus more suitable for optoelectronic device applications.[6] This family of 2D layered halide perovskites has a general formula of $(RNH_3)_2(A)_{N-1}B_NX_{3N+1}$, where R is a long chain alkyl or aromatic group, A is a monovalent cation, B is a bivalent metal

Dr. J. Wang, J. Li, S. Lan, C. Fang, H. Shen, Prof. X. Wen
School of Optical and Electronic Information
Huazhong University of Science and Technology
Wuhan 430074, P. R. China
Dr. Y. Mi, Prof. X. Liu
CAS Key Laboratory of Standardization and Measurement
for Nanotechnology
CAS Center for Excellence in Nanoscience
National Center for Nanoscience and Technology
Beijing 100190, P. R. China
E-mail: liuxf@nanoctr.cn

Dr. X. Gao, Prof. R. Chen
Department of Electrical and Electronic Engineering
Southern University of Science and Technology
Shenzhen, Guangdong 518055, P. R. China
J. Li, Prof. T. He
College of Physics and Energy
Shenzhen University
Shenzhen, Guangdong 518060, P. R. China
E-mail: tche@szu.edu.cn
Prof. D. Li
School of Optical and Electronic Information and Wuhan
National Laboratory for Optoelectronics
Huazhong University of Science and Technology
Wuhan 430074, P. R. China
E-mail: dehuili@hust.edu.cn

**ADVANCED
SCIENCE NEWS**
www.advancedsciencenews.com

**ADVANCED
OPTICAL
MATERIALS**
www.advopticalmat.de

cation, X is a halide anion, and N is the number of the inorganic layers between the adjacent two layers of the organic chains.[7] In addition to their environmental stability, 2D perovskites are equipped with tunable bandgap in the entire visible range by changing the layer number N or chemical compositions. The dielectric and quantum confinement effect in 2D layered perovskites not only lead to the large exciton binding energy, but also to enhanced optical nonlinearity.[8] The enhanced nonlinear refraction n_2 and nonlinear absorption coefficient provide the capabilities of high-power/high-efficiency NLO applications.[9]

Previous studies on the nonlinearity of 2D perovskites mainly focus on the thin films or bulk crystals. It is well known that the optical nonlinearity is highly dependent on the sample structure and symmetry.[10] We expect that the NLO properties can be also greatly enhanced in heterostructural 2D perovskites; nonetheless, studies on this have not been explored yet. Here, we systematically explore the NLO properties of $(n\text{-}C_4H_9NH_3)_2PbI_4/(n\text{-}C_4H_9NH_3)_2(CH_3NH_3)Pb_2I_7$ (denoted as $(BA)_2PbI_4/(BA)_2MAPb_2I_7$) heterostructures, which were synthesized according to the method we developed previously. The centimeter size, high phase purity, and high crystalline quality of the as-synthesized heterostructures provide the capability to obtain high NLO response. Two/three-photon-absorption (2PA/3PA) and 2PA-/3PA-induced photoluminescence (PL) were successfully observed. In addition, the nonlinear transmittance measurement revealed that the 2PA coefficient highly depends on sample thickness and a giant two-photon absorption coefficient of 44 cm MW^{-1} was achieved for the heterostructures with a total thickness of 20 μm. The 2PA coefficients of our heterostructures are overall several orders of magnitude larger than the other materials.[11] Furthermore, direct photodetection of near infrared light (980 nm) was demonstrated with a responsivity on the order of 10^{-7} A W^{-1} under an applied voltage of 1 V due to the high 2PA coefficient in our heterostructures. The demonstration of direct infrared photodetections in 2D halide perovskite heterostructures provides a possible alternative in advanced integrated optoelectronics.

2. Results and Discussion

2D perovskite heterostructures with centimeter size were synthesized according to our previous report.[12] As shown in **Figure 1**a, in contrast to 3D MAPbI$_3$ (n) which crystallizes in the tetragonal I4/mcm space group at room temperature, 2D perovskites exhibit the orthorhombic space groups *Pcab* for $(BA)_2PbI_4$ (N 1) and *Ccmm* for $(BA)_2MAPb_2I_7$ (N 2), respectively (Table S1, Supporting Information).[13] The heterostructures were constructed by sandwiching N 1 by two layers of N 2 as shown in Figure 1b. It should be noted that our synthetic method cannot grow perovskite heterostructure single crystals with regularly alternating N 1 and N 2 blocks in a periodic manner. Figure 1c displays the optical image of an as-synthesized 2D perovskite heterostructure with a lateral size of about 2 cm which is big enough for our measurements. X-ray diffraction (XRD) patterns of the synthesized plates show that all diffraction peaks can be well-indexed to (00k) peaks of N 1 and (0k0) peaks of N 2, suggesting the high phase purity and high crystalline quality of the heterostructures (Figure 1d).[6b,14] For comparison, the XRD diffraction patterns of pure N 1
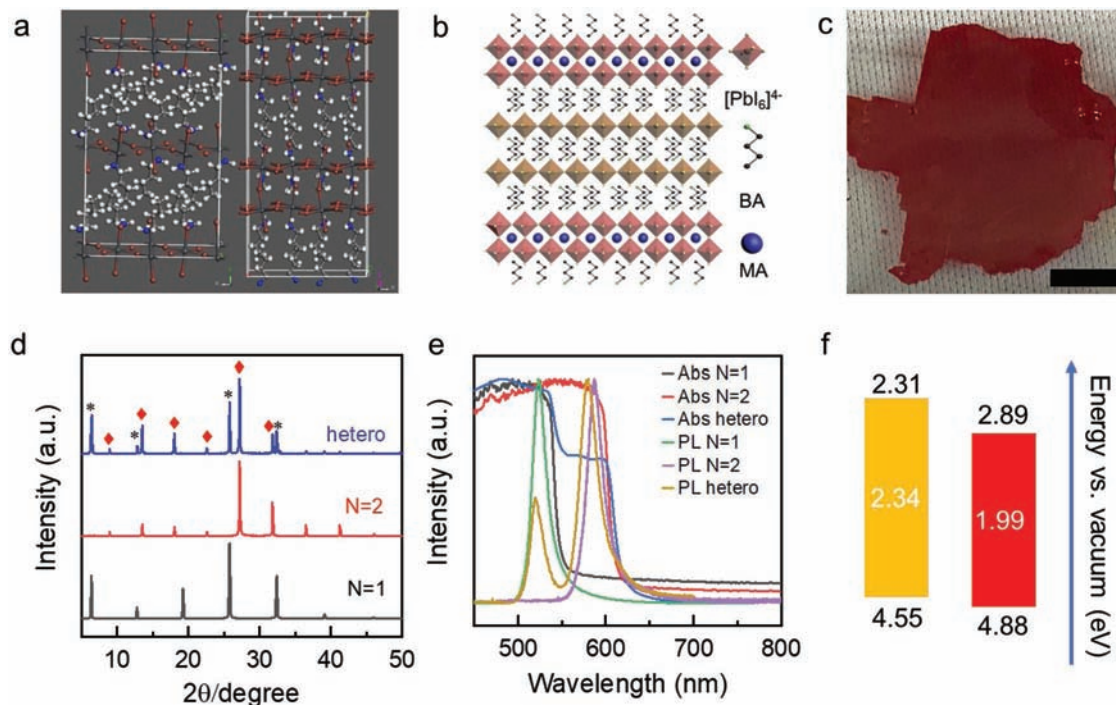

Figure 1. a) Schematic illustration of the crystal structure of N 1 and N 2. b) Schematic illustration of N 1/N 2 heterostructure. c) Optical image of N 1/N 2 heterostructure. The scale bar is 0.5 cm. d) XRD patterns of N 1, N 2 and N 1/N 2 heterostructure. e) Normalized PL spectra and absorption of N 1/N 2 heterostructure together with the normalized PL and absorption spectra of N 1 and N 2 crystals. f) Band diagram of the corresponding N 1/N 2 heterostructure.

and N 2 2D perovskites synthesized by solution method are also given in Figure 1d and we also summarize the XRD diffraction peak positions of N 1 and N 2 2D perovskites (Tables S2 and S3, Supporting Information). The absorption spectrum exhibits absorption edges at 530 and 623 nm, corresponding to the excitonic absorption of N 1 and N 2, respectively. The room-temperature PL spectra (Figure 1e) of the heterostructure also verifies the formation of the N 1/N 2 heterostructures, where two emission peaks at 520 and 590 nm are consistent with the excitonic emission of the N 1 and N 2 2D perovskite films, respectively.[15] The optical image of individual N 1 and N 2 plates are also given for comparisons (Figure S1, Supporting Information). The band alignment diagram of the heterostructures is shown in Figure 1f according to the previous X-ray photoelectron spectroscopy (XPS) studies, which can be classified as the type-II structure.[6b] This sort of band alignment favors the photogenerated carrier separation and thus enhances the photodetection efficiency.

The Z-scan technique has been widely used to determine the nonlinear refraction n_2 and nonlinear absorption coefficient .[16] However, it was found that the nonuniform thickness, nonlinearity inhomogeneities, and nonf at surfaces of nonlinear materials would significantly distort the closed Z-scan curves.[17] Consequently, the Z-scan method is not a practical choice to measure the third-order nonlinear susceptibility of the inhomogeneous samples.[18] Therefore, we have carried out the nonlinear transmittance measurements at fixed spots to extract the nonlinear optical parameters. This technique has the advantages of conveniently choosing measurement positions and excluding the influence of inhomogeneity of the samples. In our experiments, each measurement was repeated at least three times on the same spot to confirm that the sample was not damaged.

Figure 2a illustrates the schematic of the nonlinear transmittance measurement setup. The excitation laser was split into identical reference and sample beam, which were used for calibration and sample characterization, respectively.[19] A power attenuator was added to tune the power of pump laser. The excitation source is a spatially Gaussian shaped, 100 fs Ti: Sapphire pulse laser operating at the wavelength of 800 nm with a repetition rate of 1 kHz. The laser beam was focused to a waist radius of 35 μm by a lens with a focal length of 50 cm. For comparisons, the nonlinear transmittance measurements of the samples of N 1 and N 2 were first conducted (Figure 2b,c). Figure 2d–g show the results of nonlinear transmittance measurements of several heterostructure samples with different thickness. The XRD patterns for those samples are also exhibited, which confirm the crystal phase purity of the used samples (Figure S2, Supporting Information).

The 2PA saturation theory was utilized to fit the experimental data in Figure 2b–g to extract nonlinear absorption coefficient and saturated absorption intensity I_{sat}. In NLO materials, the intensity of incident light after propagating through a two-photon absorbing medium is given by the following differential equation[3c,20]

$$\frac{dI(z)}{dz} = -\alpha_0 I(z) - \beta(I)I^2(z) \tag{1}$$

where $I(z)$ is the light intensity at the propagation distance z in the sample, $_0$ is the linear absorption coefficient, and (I) is the intensity-dependent 2PA coefficient. Considering the intensity reduction due to the possible reflection and scattering when light passes the sample, particularly for our heterostructures, an accurate expression for the normalized transmission can be expressed as[21]
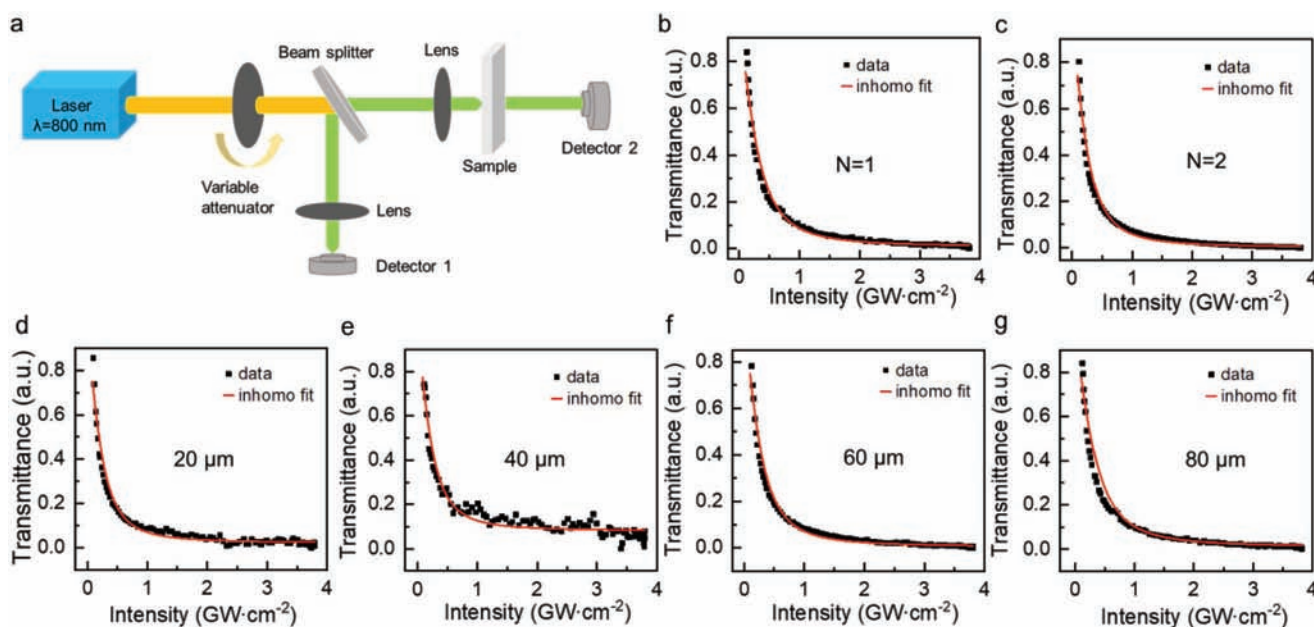

Figure 2. a) Schematic diagram of the setup of nonlinear transmittance measurement. b,c) Nonlinear transmittance versus peak intensity of incident laser for N 1 and N 2 plates, respectively. d–g) Nonlinear transmittance versus peak intensity of incident laser for N 1/N 2 heterostructures with different thicknesses. For all figures (b)–(g), the dots are experimental data and the lines denote fitting results obtained from the inhomogeneous saturation model.

$$T(I) = \frac{(1-R)^2 e^{-a_0 L}}{(1-R)\beta I L_{eff} + 1} \qquad (2)$$

where L_{eff} [1 − exp(− $_0L$)]/ $_0$ is the effective length of the sample, L is the thickness of the sample measured, R $(n_1 - n_2)^2/(n_1 + n_2)^2$ represents the reduction factor caused by the reflection and scattering, n_1 is linear refraction index of the sample, while n_2 is the linear refraction index of the substrate that is 1.544 for quartz. For our heterostructures that contain both N 1 and N 2 2D perovskites, the effective $_0$ and n_1 were used when it comes to different thickness of N 1 and N 2 layers (Note S1, Supporting Information).

When 2PA saturation occurs, the nonlinear absorption coefficient is supposed to be dependent on the irradiance. Four different models can be utilized to extract and I_{sat}, which are constant model, hyperbolic saturation model, homogeneous saturation model, and inhomogeneous saturation model (Note S2, Supporting Information). The experimental data in Figure 2b–g can be well fitted by combining inhomogeneous saturation model with Equation (2) (Figure S3, Supporting Information).[22] This is expected since while hyperbolic saturation model can be applied in the pure phase semiconductors without doping, the inhomogeneous saturation model is more appropriate to the doped semiconductors with nonuniform characteristics.[16a,23] Therefore, in our heterostructures that consist of different materials, the inhomogeneous saturation model gives better fittings (Figure S3, Supporting Information). The fitting results of the 2PA coefficient $_0$ and 2PA saturation intensity I_{sat} for plates with different thicknesses are displayed in **Figure 3**. Both $_0$ and I_{sat} of the heterostructures show a strong thickness dependence. As the thickness of the heterostructures increases from 20 to 80 μm, $_0$ reduces from 44.0 to 8.57 cm MW^{-1} while I_{sat} increases from 0.326 to 0.468 GW cm^{-2}. This thickness-dependent 2PA is of great significance for designing high-performance devices by selecting sample with a proper thickness.[24]

For comparisons, we have summarized the nonlinear absorption coefficient $_0$ and saturated absorption intensity I_{sat} of different nanostructures in **Table 1**, including II–VI semico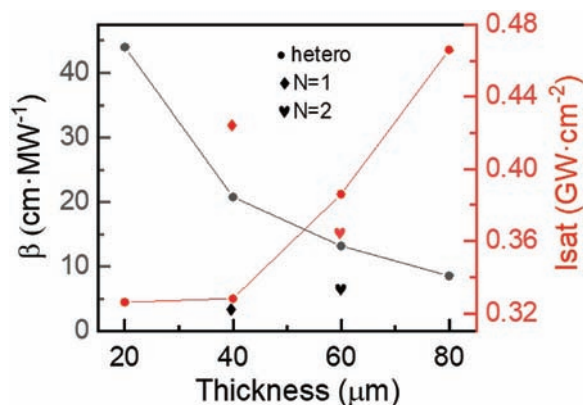nducting nanocrystals, monolayer 2D transition metal dichalcogenides, KTP single crystals, all-inorganic 3D QDs, perovskite powder, mechanically exfoliated 2D perovskite flakes, and 2D/3D perovskite films.[3b,20,23b,25] Among all of them, the nonlinear absorption coefficients of our heterostructure are overall several orders of magnitude larger than the other materials and around five times smaller than that of 1 μm thick (PEA)$_2$PbI$_4$ flake obtained by mechanical exfoliation.[20] Compared with $_0$ of pure N 1 (4.56 cm MW^{-1}) and N 2 (6.25 cm MW^{-1}) 2D perovskite crystals (Figure 3), the enhanced nonlinear absorption coefficients in our 2D heterostructures might be attributed to the small thickness of N 2 layer, the enhanced nonradiative energy transfer, and excellent crystalline quality of our heterostructures.[11b,26] The thickness of N 2 layer is around 1 μm in our synthesized heterostructures with a total thickness of 20 μm. It was reported $_0$ can dramatically increase with the decrease of the thickness. In addition, the nonradiative energy transfer from N 1 layer to N 2 layer via an antenna-like effect might further enhance $_0$ while the defect effect can be minimized in our high crystalline quality heterostructures and thus can also increase $_0$.[27] All those factors together result in the large $_0$ in our heterostructures.

In view of the giant 2PA coefficient and strong emission in our 2D perovskite heterostructures, we expect that multiphoton-induced photoluminescence (MPL) would be present as well.[28] As shown in Figure 1f, the exciton emission energies of the pure N 1 and N 2 perovskites are 2.34 eV (530 nm) and 1.99 eV (623 nm), respectively.[29] The energy range of the excitation photon capable of inducing the two-photon-induced photoluminescence (2PL) is 1.17 $\hbar$ 2.34 eV (1060 530 nm) for N 1 and 0.995 $\hbar$ 1.99 eV (1246 623 nm) for N 2, respectively. **Figure 4**a displays the schematic illustration of 2PL process while Figure 4b shows a typical power-dependent 2PL spectra of a typical heterostructure with a thickness of 60 μm excited by a 800 nm, 100 fs pulse laser with 1 kHz repetition. The high energy emission peak can be ascribed to the 2PL of N 1 layer while the low energy emission peak is due to the 2PL of N 2 outer layer, both of which are consistent with emission peaks in PL spectra (Figure 1e). The excitation power-dependent integrated emission intensity for both peaks extracted from Figure 4b can be well fitted by a quadratic function (Figure 4c,d), further confirming that those two emission peaks indeed originate from the 2PL of N 1 and N 2 layers, respectively.

To investigate MPL in our heterostructures, we switched the excitation wavelength from 800 to 1200 nm, which allows the 3PA in N 1 layer while 2PA in N 2 layers due to the different bandgap energy (Figure 4e). Similarly, under 1200 nm excitation, two emission peaks were observed in our heterostructures corresponding to N 1 and N 2 layers, respectively (Figure 4f). The excitation power-dependent integrated emission intensity extracted from Figure 4f exhibit a cubic and quadratic dependence for N 1 and N 2, respectively (Figure 4g,h). As expected, we can conclude that it is 3PA-induced PL for N 1 inner layer and 2PL for N 2 outer layers in our heterostructures under 1200 nm excitation. It should be noted that for all N 1, N 2 2D perovskite crystals and N 1/N 2 heterostructures, the emission peaks show a gradual redshift as the excitation wavelength change from 473 to 800 nm and finally to 1200 nm (Figure S4, Supporting Information). This

Figure 3. Thickness-dependent 2PA coefficient and 2PA saturation intensity for N 1/N 2 heterostructures. For comparison, the results of N 1 (4.56 cm MW^{-1}, 40 μm) and N 2 (6.25 cm MW^{-1}, 60 μm) are included as well.

Table 1. The nonlinear absorption parameters for different nanostructures.

Material	E_g	[nm]	Pulse	[cm MW^{-1}]	I_{sat} [GW cm^{-2}]
KH$_2$PO$_4$ single crystal	3.35	532	–	0.24 10^{-3}	–
WS$_2$ monolayer	1.95	800	40 fs, 1 kHz	0.52	–
CdS nanocrystals	2.71	780	120 fs, 1 kHz	11 10^{-3}	190
CH$_3$NH$_3$PbI$_3$ single crystal	1.45	1064	30 ps, 50 Hz	23 10^{-3}	–
CH$_3$NH$_3$PbI$_3$ film	1.61	1064	40 ps	−2.25	12.71
(PEA)$_2$PbI$_4$ film	2.40	800	100 fs, 1 kHz	12.6	0.22
CsPbBr$_3$ nanocrystal	2.38	800	100 fs, 1 kHz	−0.68 10^{-3}	0.011
(PEA)$_2$PbI$_4$ nanosheet	2.40	800	100 fs, 1 kHz	211.5	0.21
(BA)$_2$(FA)Pb$_2$Br$_7$ film	2.37	1030	350 fs, 100 Hz	5.67	–
(BA)$_2$PbI$_4$ powder	2.43	1060	30 ps, 50 Hz	15.3 10^{-3}	0.19
(BA)$_2$MAPb$_2$I$_7$ powder	1.99			18.4 10^{-3}	0.18
(BA)$_2$PbI$_4$/(BA)$_2$MAPb$_2$I$_7$ heterostructure	–	800	100 fs, 1 kHz	44.0	0.33

is believed to be due to the reabsorption effect according to previous reports.[30]

Infrared light harvesting and detection is of great importance for various optoelectronic devices, such as solar cells and photodetectors.[31] As for solar cells, the ability of harvesting infrared light can make full use of both visible and infrared light in the solar spectrum, and thus enhance the PCE.[2b] In terms of the photodetectors, the higher infrared light absorption coefficient can enhance the performance and sensitivity of infrared light detection.[32] Our 2D perovskite heterostructures with a giant multiphoton absorption coefficient are promising for the infrared photodetector applications.

We have successfully demonstrated an infrared photodetector based on our 2D perovskite heterostructures. The device schematics is illustrated in the inset picture in **Figure 5**a. An indium tin oxide (ITO) substrate serves as the bottom electrode while a 100 nm Au/10 nm Cr layer was deposited on the top to serve as the top electrode. The infrared light was incident from the bottom ITO substrate. The *I–V* characteristics of the 2D perovskite heterostructure device under dark and a 980 nm laser irradiation with different power were plotted in Figure 5a. Taking the advantages of the high crystalline quality and low intrinsic carrier concentration of our heterostructures, the dark current is extremely small, on the order of 10^{-12} A. When
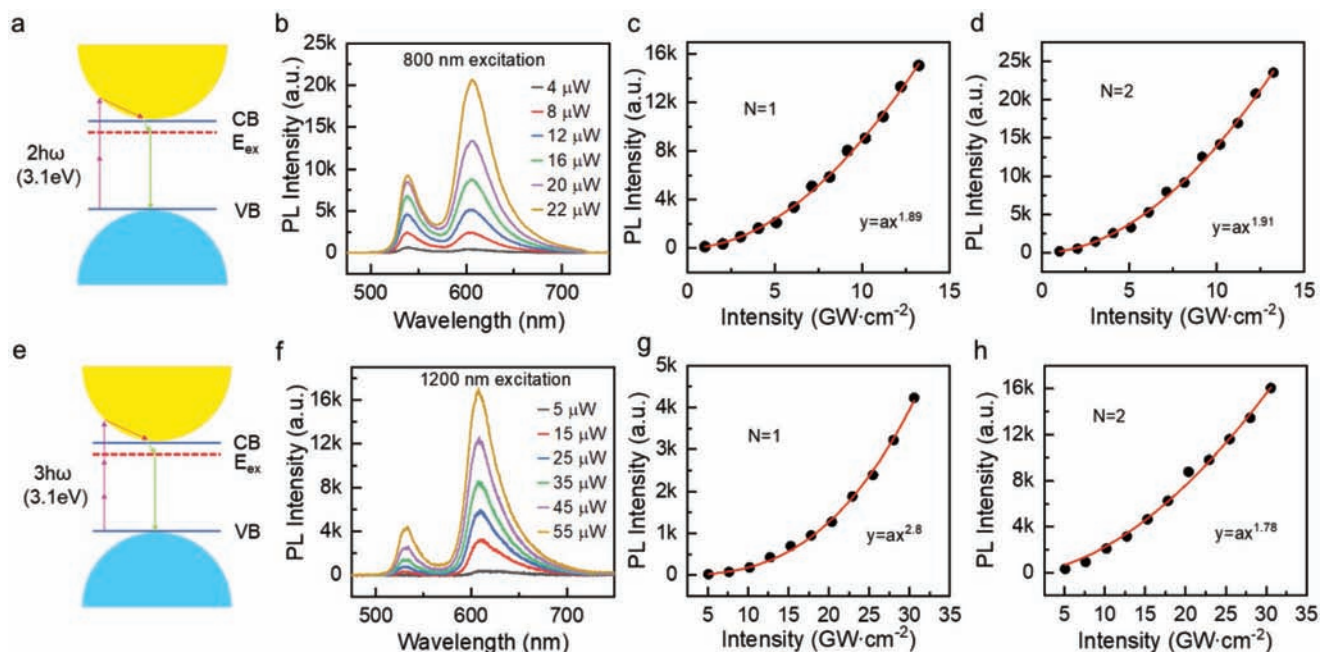

Figure 4. a) Schematic of 2PL. b) Emission spectra of N 1/N 2 heterostructure under a 800 nm excitation. c,d) Extracted incident power-dependent emission intensity under a 800 nm excitation for N 1 and N 2, respectively. The solid lines are fitting results based on a quadratic function. e) Schematic of 3PL. f) Emission spectra of N 1/N 2 heterostructure under a 1200 nm excitation. g,h) Extracted incident power-dependent emission intensity under a 1200 nm excitation for N 1 and N 2, respectively. The solid lines are fitting results based on a quadratic function and cubic function.
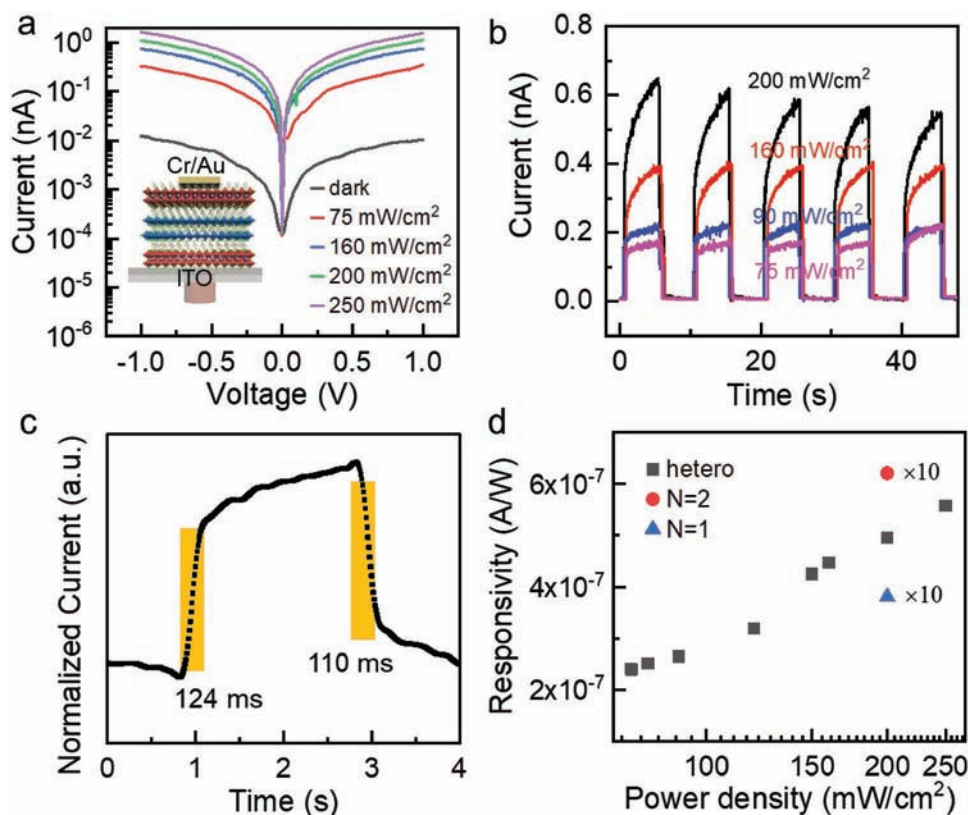
Figure 5. a) The *I–V* characteristics of the 2D perovskite heterostructure device with a thickness of 20 µm in dark and under a 980 nm laser irradiation with different powers. Inset is schematic of the photodetector based on the N 1/N 2 heterostructure. b) Switch characteristics of the device under different light powers at a bias of 1 V. c) Temporal photoresponse of the N 1/N 2 heterostructure device illuminated by a 980 nm light under a bias of 1 V. d) The responsivity as a function of the illumination power density under a bias of 1 V.

the 980 nm laser was turned on, the photocurrent increased significantly, attributing to the strong 2PA in our heterostructures as discussed above. For comparison, the photodetection of bare ITO substrate was also investigated, which shows no response to 980 nm light (Figure S5, Supporting Information). Previous reports show that second harmonic generation has been demonstrated in bilayer WSe_2 excited by a CW 1064 nm laser.[33] Therefore, it is reasonable to observe nonlinear effect under a CW laser excitation in view of the much large nonlinear effect in 2D perovskites compared with that in WSe_2.[21] For comparison, *I–V* curves of the N 1 and N 2 photodetectors were shown in Figure S6 in the Supporting Information.

Figure 5b displays temporal response measurements under different illumination power at a bias of 1 V, suggesting the excellent reversibility and repeatability of our heterostructural devices. The extracted current-on/off ratio can reach around 10^3 for the incident power density of 200 mW cm^{-2} at a bias of 1 V. The response speed, characterized by rise time and decay time, is an important parameter for the photodetectors and optical switches. The extracted rise time (from 10% to 90% of the peak value) was 124 ms, and decay time (from 90% to 10% peak value) was 110 ms (Figure 5c), comparable to that working in single photon absorption range.[6c,32]

The responsivity (*R*) is another important parameter used to evaluate the performance of a photodetector and defined as R I_{photo}/P, where I_{photo} is photocurrent and *P* is the light

power illuminated on device. The responsivity as a function of the illumination power indicates that the responsivity increases almost linearly with the increase of illumination intensity (Figure 5d). This linear increase of *R* with the illumination intensity further verifies that the photocurrent is primary due to the direct two-photon absorption rather than the thermal effect or defect related upconversion.[31,34] The responsivity is on the order of 10^{-7} A W^{-1} under an applied voltage of 1 V, which is comparable with the responsivity of single-crystalline perovskite $CH_3NH_3PbBr_3$ photodetector working at 800 nm,[3a] $CH_3NH_3Pb_{0.75}Sn_{0.25}I_3$ thin film (linear absorption over 900 nm) photodetector at 1064 nm,[35] and well-designed perovskite-erbium silicate nanosheet hybrid waveguide photodetector at 1530–1560 nm (Table S4, Supporting Information).[31] For comparison, the responsivity of pure N 1 and N 2 plates is included in Figure 5d (Figure S7, Supporting Information), which is one order of magnitude smaller than that in our heterostructures. This is because that the 2PA coefficient of heterostructures is much higher than a single component as we discussed above (Figure 3).

Heterostructures consisting of two or more materials with different energy landscape exhibit several advantages in terms of their nonlinear optical properties compared with single material system. First, heterostructures exhibit new physical phenomena inaccessible to the single material system and can greatly extend their functionalities for novel electronic and

optoelectronic applications. For the nonlinear optical applications of our heterostructures, we can properly select the excitation wavelength so that different order nonlinear effect takes place in N 1 and N 2. In such way, heterostructures provide an extra degree of freedom to tune the emission wavelength for special applications or can realize dual-band emission or detection. Second, either the total thickness of the heterostructures or the thickness of the constituting layers can be well tuned so that the 2PA coefficient $_0$ and saturation intensity I_{sat} could be efficiently modulated in a wider range. This thickness-dependent 2PA is of great significance for designing high-performance devices by selecting proper thickness of the heterostructures. Third, it has been demonstrated that the presence of the nonradiative energy transfer and internal electrical field at the interfaces would greatly enhance the nonlinear effect in heterostructures.[11a,27]

3. Conclusion

In conclusion, NLO properties of 2D perovskite heterostructures have been investigated by nonlinear transmittance and MPL measurements. The heterostructures exhibit a strong thickness-dependent nonlinearity and a giant 2PA coefficient of 44 cm MW^{-1} was achieved when the total thickness of the heterostructure is 20 μm. The origin of the giant nonlinearity in our heterostructures might be attributed to the small thickness of the N 2 layers as well as the nonradiative energy transfer within the heterostructures. Owing to the high multiphoton absorption coefficients, strong MPL was observed in our heterostructures. In addition, an infrared photodetector based on our heterostructures has been demonstrated with a responsivity of 10^{-7} A W^{-1} benefiting from the giant 2PA coefficient. Our studies provide a strategy to enhance the nonlinearity of 2D perovskites via constructing a heterostructure. The giant multiphoton absorption coefficient of our heterostructures also suggests the promising applications in infrared light detections and other NLO devices.

4. Experimental Section

Synthesis of Centimeter-Size 2D Perovskite Heterostructure Plates: 2D perovskite heterostructure single-crystal with different thickness was synthesized according to the previous work.[12] 0.45 g PbO powder was dissolved in a mixture of 3.5 mL HI (57% w/w aqueous) and 0.5 mL H$_3$PO$_2$ (50% w/w aqueous) by heating at 150 C under constant magnetic stirring. Then 1.75 mol L^{-1} BAI solution was added into the resultant solution and slowly cooled down to 75 C while 0.15 g MAI powder was successively injected into the solution for the synthesis of (BA)$_2$(MA)PbI$_4$/(BA)$_2$(MA)Pb$_2$I$_7$ plates. For different thickness of the heterostructures, the MAI concentration of the reaction solution changes from 0.25 to 1 mol L^{-1} but with a fixed BAI to MAI ratio of 2:3 while maintaining other conditions the same. The synthesis was carried out in ambient conditions with a relative humidity of 50%.

Material Characterizations: Powder X-ray diffraction measurements were recorded using a Bruker D2 PHASER (Cu K 0.15419 nm, Nickel filter, 25 kV, 40 mA). The linear absorption spectra were recorded on an ultraviolet–vis spectrophotometer (UV-1750, SHIMADZU). The linear photoluminescence measurements were performed in backscattering configuration using a Horiba HR550 system equipped with a 600 g mm^{-1} grating excited by a 473 nm solid-state laser with a

power of 1 μW. The objective used was 50 and the diameter of beam spot is around 2 μm for PL measurement.

Infrared Photodetector Measurement: 10 nm Cr/100 nm Au electrodes were defined by a shadow mask and deposited by electron beam evaporation. The incident light intensity was recorded by a pyroelectric detector (Gentec, model APM (D)). The photocurrent was collected by a lock-in amplifier (Stanford SR830) coupled with a mechanical chopper while the response speed was acquired on a digital oscilloscope (Tektronix MDO3032). All measurements were performed in ambient atmosphere.

Supporting Information

Supporting Information is available from the Wiley Online Library or from the author.

Conflict of Interest

The authors declare no conflict of interest.

[1] a) N.-G. Park, *Mater. Today* **2015**, *18*, 65; b) H. J. Snaith, *Nat. Mater.* **2018**, *17*, 372; c) M. A. Green, A. Ho-Baillie, H. J. Snaith, *Nat. Photonics* **2014**, *8*, 506.

[2] a) R. J. Sutton, G. E. Eperon, L. Miranda, E. S. Parrott, B. A. Kamino, J. B. Patel, M. T. Hörantner, M. B. Johnston, A. A. Haghighirad, D. T. Moore, *Adv. Energy Mater.* **2016**, *6*, 1502458; b) Q. Zhang, R. Su, X. Liu, J. Xing, T. C. Sum, Q. Xiong, *Adv. Funct. Mater.* **2016**, *26*, 6238; c) Y. Liu, Y. Zhang, Z. Yang, H. Ye, J. Feng, Z. Xu, X. Zhang, R. Munir, J. Liu, P. Zuo, Q. Li, M. Hu, L. Meng, K. Wang, D. M. Smilgies, G. Zhao, H. Xu, Z. Yang, A. Amassian, J. Li, K. Zhao, S. F. Liu, *Nat. Commun.* **2018**, *9*, 5302; d) K. Lin, J. Xing, L. N. Quan, F. P. G. de Arquer, X. Gong, J. Lu, L. Xie, W. Zhao, D. Zhang, C. Yan, W. Li, X. Liu, Y. Lu, J. Kirman, E. H. Sargent, Q. Xiong, Z. Wei, *Nature* **2018**, *562*, 245.

[3] a) G. Walters, B. R. Hoogland, S. Hoogland, D. Shi, R. Comin, D. P. Sellan, O. M. Bakr, E. H. Sargent, *ACS Nano* **2015**, *9*, 9340; b) R. Zhang, J. Fan, X. Zhang, H. Yu, H. Zhang, Y. Mai, T. Xu,

ADVANCED
SCIENCE NEWS

www.advancedsciencenews.com

ADVANCED
OPTICAL
MATERIALS

www.advopticalmat.de

J. Wang, H. J. Snaith, *ACS Photonics* **2016**, *3*, 371; c) T. He, J. Li, C. Ren, S. Xiao, Y. Li, R. Chen, X. Lin, *Appl. Phys. Lett.* **2017**, *111*, 211105.

[4] A. Ferrando, J. P. Martinez Pastor, I. Suarez, *J. Phys. Chem. Lett.* **2018**, *9*, 5612.

[5] a) L. Wang, N. E. Williams, E. W. Malachosky, J. P. Otto, D. Hayes, R. E. Wood, P. Guyot-Sionnest, G. S. Engel, *ACS Nano* **2017**, *11*, 2689; b) Z. Wang, Q. Lin, F. P. Chmiel, N. Sakai, L. M. Herz, H. J. Snaith, *Nat. Energy* **2017**, *2*, 17135.

[6] a) M. D. Smith, E. J. Crace, A. Jaffe, H. I. Karunadasa, *Annu. Rev. Mater. Res.* **2018**, *48*, 111; b) D. H. Cao, C. C. Stoumpos, O. K. Farha, J. T. Hupp, M. G. Kanatzidis, *J. Am. Chem. Soc.* **2015**, *137*, 7843; c) Y. Chen, Y. Sun, J. Peng, J. Tang, K. Zheng, Z. Liang, *Adv. Mater.* **2018**, *30*, 1703487; d) L. N. Quan, Y. Zhao, F. P. G. de Arquer, R. Sabatini, G. Walters, O. Voznyy, R. Comin, Y. Li, J. Z. Fan, H. Tan, J. Pan, M. Yuan, O. M. Bakr, Z. Lu, D. H. Kim, E. H. Sargent, *Nano Lett.* **2017**, *17*, 3701.

[7] a) J. Wang, J. Z. Li, Q. Tang, L. Li, J. B. Zhang, J. F. Zhang, P. H. Tan, J. Zhang, D. H. Li, *J. Phys. Chem. Lett.* **2017**, *8*, 6211; b) C. C. Stoumpos, D. H. Cao, D. J. Clark, J. Young, J. M. Rondinelli, J. I. Jang, J. T. Hupp, M. G. Kanatzidis, *Chem. Mater.* **2016**, *28*, 2852.

[8] a) B. Traore, L. Pedesseau, L. Assam, X. Che, J. C. Blancon, H. Tsai, W. Nie, C. C. Stoumpos, M. G. Kanatzidis, S. Tretiak, A. D. Mohite, J. Even, M. Kepenekian, C. Katan, *ACS Nano* **2018**, *12*, 3321; b) W. Chen, S. Bhaumik, S. A. Veldhuis, G. Xing, Q. Xu, M. Gratzel, S. Mhaisalkar, N. Mathews, T. C. Sum, *Nat. Commun.* **2017**, *8*, 15198.

[9] a) S. Lu, F. Zhou, Q. Zhang, G. Eda, W. Ji, *Adv. Sci.* **2018**, *6*, 1801626; b) F. O. Saouma, C. C. Stoumpos, J. Wong, M. G. Kanatzidis, J. I. Jang, *Nat. Commun.* **2017**, *8*, 742.

[10] a) R. Li, Z. Wei, H. Zhao, H. Yu, X. Fang, D. Fang, J. Li, T. He, R. Chen, X. J. Wang, *Nanoscale* **2018**, *10*, 22766; b) Y. Wang, X. Li, X. Zhao, L. Xiao, H. Zeng, H. Sun, *Nano Lett.* **2015**, *16*, 448.

[11] a) J. Xu, X. Li, J. Xiong, C. Yuan, S. Semin, T. Rasing, X. H. Bu, *Adv. Mater.* **2019**, https://doi.org/10.1002/adma.201806736; b) W. Chen, S. Bhaumik, S. A. Veldhuis, G. Xing, Q. Xu, M. Gratzel, S. Mhaisalkar, N. Mathews, T. C. Sum, *Nat. Commun.* **2017**, *8*, 15198.

[12] J. Wang, J. Li, S. Lan, C. Fang, H. Shen, Q. Xiong, D. Li, *ACS Nano* **2019**, https://doi.org/10.1021/acsnano.9b00259.

[13] a) H. Tsai, W. Nie, J. C. Blancon, C. C. Stoumpos, R. Asadpour, B. Harutyunyan, A. J. Neukirch, R. Verduzco, J. J. Crochet, S. Tretiak, L. Pedesseau, J. Even, M. A. Alam, G. Gupta, J. Lou, P. M. Ajayan, M. J. Bedzyk, M. G. Kanatzidis, *Nature* **2016**, *536*, 312; b) T. Ishihara, J. Takahashi, T. Goto, *Phys. Rev. B* **1990**, *42*, 11099.

[14] C. Fang, J. Li, J. Wang, R. Chen, H. Wang, S. Lan, Y. Xuan, H. Luo, P. Fei, D. Li, *CrystEngComm* **2018**, *20*, 6538.

[15] a) J. Yan, W. Qiu, G. Wu, P. Heremans, H. Chen, *J. Mater. Chem. A* **2018**, *6*, 111063; b) Y. Chen, S. Yu, Y. Sun, Z. Liang, *J. Phys. Chem. Lett.* **2018**, *9*, 2627.

[16] a) B. Gu, Y.-X. Fan, J. Chen, H.-T. Wang, J. He, W. Ji, *J. Appl. Phys.* **2007**, *102*, 083101; b) X. Zheng, Y. Zhang, R. Chen, X. Cheng, Z. Xu, T. Jiang, *Opt. Express* **2015**, *23*, 15616.

[17] Q. Yang, J. Seo, S. Creekmore, D. Temple, A. Mott, N. Min, K. Yoo, S. Y. Kim, S. Jung, *Appl. Phys. Lett.* **2003**, *82*, 19.

[18] F. O. Saouma, D. Y. Park, S. H. Kim, M. S. Jeong, J. I. Jang, *Chem. Mater.* **2017**, *29*, 6876.

[19] R. I. Woodward, R. C. T. Howe, G. Hu, F. Torrisi, M. Zhang, T. Hasan, E. J. R. Kelleher, *Photonics Res.* **2015**, *3*, A30.

[20] W. Liu, J. Xing, J. Zhao, X. Wen, K. Wang, P. Lu, Q. Xiong, *Adv. Opt. Mater.* **2017**, *5*, 1601045.

[21] M. Rumi, J. W. Perry, *Adv. Opt. Photonics* **2010**, *2*, 451.

[22] a) N. Dong, Y. Li, S. Zhang, N. McEvoy, R. Gatensby, G. S. Duesberg, J. Wang, *ACS Photonics* **2018**, *5*, 1558; b) Y. Li, N. Dong, S. Zhang, X. Zhang, Y. Feng, K. Wang, L. Zhang, J. Wang, *Laser Photonics Rev.* **2015**, *9*, 427.

[23] a) J. Lami, P. Gilliot, C. Hirlimann, *Phys. Rev. Lett.* **1996**, *77*, 1632; b) D. Sun, Y. Rao, G. A. Reider, G. Chen, Y. You, L. Brézin, A. R. Harutyunyan, T. F. Heinz, *Nano Lett.* **2014**, *14*, 5625.

[24] J. Zhang, T. Jiang, X. Zheng, C. Shen, X. Cheng, *Opt. Lett.* **2017**, *42*, 3371.

[25] a) T. Xu, F. Chen, S. Dai, X. Shen, X. Wang, Q. Nie, C. Liu, K. Xu, J. Heo, *J. Non-Cryst. Solids* **2011**, *357*, 2219; b) M. He, C. Quan, C. He, Y. Huang, L. Zhu, Z. Yao, S. Zhang, J. Bai, X. Xu, *J. Phys. Chem. C* **2017**, *121*, 27147; c) K. N. Krishnakanth, S. Seth, A. Samanta, S. V. Rao, *Opt. Lett.* **2018**, *43*, 603; d) Y. Gao, S. Wang, C. Huang, N. Yi, K. Wang, S. Xiao, Q. Song, *Sci. Rep.* **2017**, *7*, 45391; e) L. Li, X. Shang, S. Wang, N. Dong, C. Ji, X. Chen, S. Zhao, J. Wang, Z. Sun, M. Hong, J. Luo, *J. Am. Chem. Soc.* **2018**, *140*, 6806.

[26] S. Chen, C. Teng, M. Zhang, Y. Li, D. Xie, G. Shi, *Adv. Mater.* **2016**, *28*, 5969.

[27] a) T. He, R. Chen, Z. B. Lim, D. Rajwar, L. Ma, Y. Wang, Y. Gao, A. C. Grimsdale, H. Sun, *Adv. Opt. Mater.* **2014**, *2*, 40; b) G. Xing, S. Chakrabortty, K. L. Chou, N. Mishra, C. H. A. Huan, Y. Chan, T. C. Sum, *Appl. Phys. Lett.* **2010**, *97*, 061112.

[28] a) T.-C. Wei, S. Mokkapati, T.-Y. Li, C.-H. Lin, G.-R. Lin, C. Jagadish, J.-H. He, *Adv. Funct. Mater.* **2018**, *28*, 1707175; b) W. Liu, X. Li, Y. Song, C. Zhang, X. Han, H. Long, B. Wang, K. Wang, P. Lu, *Adv. Funct. Mater.* **2018**, *28*, 1707550.

[29] J. Li, J. Wang, J. Ma, H. Shen, L. Li, X. Duan, D. Li, *Nat. Commun.* **2019**, *10*, 806.

[30] P. J. Guo, W. Huang, C. C. Stoumpos, L. L. Mao, J. Gong, L. Zeng, B. T. Diroll, Y. Xia, X. D. Ma, D. J. Gosztola, T. Xu, J. B. Ketterson, M. J. Bedzyk, A. Facchetti, T. J. Marks, M. G. Kanatzidis, R. D. Schaller, *Phys. Rev. Lett.* **2018**, *121*, 127401.

[31] X. Zhang, S. Yang, H. Zhou, J. Liang, H. Liu, H. Xia, X. Zhu, Y. Jiang, Q. Zhang, W. Hu, X. Zhuang, H. Liu, W. Hu, X. Wang, A. Pan, *Adv. Mater.* **2017**, *29*, 1604431.

[32] J. Song, Q. Cui, J. Li, J. Xu, Y. Wang, L. Xu, J. Xue, Y. Dong, T. Tian, H. Sun, H. Zeng, *Adv. Opt. Mater.* **2017**, *5*, 1700157.

[33] H. Yu, D. Talukdar, W. Xu, J. B. Khurgin, Q. Xiong, *Nano Lett.* **2015**, *15*, 5653.

[34] a) J. Wu, Y. T. Chun, S. Li, T. Zhang, J. Wang, P. K. Shrestha, D. Chu, *Adv. Mater.* **2018**, *30*, 1705880; b) Z. Sun, H. Chang, *ACS Nano* **2014**, *8*, 4133; c) J. Li, Y. Shen, Y. Liu, F. Shi, X. Ren, T. Niu, K. Zhao, S. F. Liu, *ACS Appl. Mater. Interfaces* **2017**, *9*, 19176.

[35] Y. Xie, J. Fan, C. Liu, S. Chi, Z. Wang, H. Yu, H. Zhang, Y. Mai, J. Wang, *Adv. Opt. Mater.* **2018**, *6*, 1700819.